Geophys. J. R. astr. Soc. (1987) **89**, 889–914

Interpretation of transient electromagnetic soundings over three-dimensional structures for the central-loop configuration

Gregory A. Newman*, Walter L. Anderson† and Gerald W. Hohmann*

* *Department of Geology and Geophysics, University of Utah, Salt Lake City, Utah 84112–1183, USA*

† *US Geological Survey, Box 25046, MS 964, Denver Federal Center, Denver, Colorado 80225, USA*

Accepted 1986 November 4. Received 1986 November 4; in original form 1986 May 12

Summary. An assessment is made of the bias of fitting constrained layered-earth models to transient electromagnetic data obtained over 3-D structures. In this assessment we use the central-loop configuration and show that accurate estimates of the depth of burial of 3-D structures can be obtained with layered-earth model fitting. However, layered-earth interpretations are not reliable for estimating depth extents and resistivities of 3-D structures. When layered earths are used for interpretation, it is advantageous in some cases to use data based on the magnetic field instead of the voltage. A magnetic-field definition of apparent resistivity, in contrast to a definition based on the voltage, eliminates apparent-resistivity overshoots and undershoots in the data. A resistivity undershoot in the data can produce an extraneous and misleading layer in an interpretation of a 3-D resistive structure. Due to 3-D effects, apparent-resistivity soundings (magnetic field and voltage) may rise so steeply at late times that it may not be possible to fit a sounding to a reasonable layered-earth model. Truncating such a sounding, over a buried conductor, allows for a reasonable layered-earth fit and an accurate estimate of the depth to the conductor. However, the resistivity of the conductor is overestimated.

Measurements of the horizontal field in the central-loop configuration can map 3-D structures, provided the sensor is located accurately at the centre of the transmitting loop. Horizontal-field calculations show that the transients peak on the flanks of a 3-D structure, but are depressed over the structure's centre. Weak transient responses flanked by two large transient responses, which are opposite in sign, locate the structure. The sign reversal is caused by a corresponding reversal in the currents that are channelled through or deflected away from conductive or resistive structures, respectively.

Key words: 3-D transient responses, apparent resistivity, layered-earth interpretation, bias, horizontal-field interpretation

1 Introduction

Transient electromagnetic (TEM) sounding is an important technique for mapping subsurface geoelectric structure (*cf.* Nabighian 1984; Frischknecht & Raab 1984; Fitterman & Stewart 1986). The central-loop sounding method is a version of the TEM sounding technique used extensively in the United States and Canada. The sounding method is illustrated in Fig. 1. A sensor placed at the centre of a square transmitting loop measures the voltage or magnetic-field response of the Earth after the current is shut off. Ideally the current is a step function, but in practice a linear-ramp shut-off is the best that can be achieved. Typical ramp lengths are of the order 0.1–1.0 ms. The sensor placed at the centre of the loop would be a coil for a voltage measurement or a squid if the magnetic field is measured. The magnetic field step-response can also be calculated from the voltage measurement (*cf.* Eaton & Hohmann 1986). The central-loop sounding method is now being used in exploration for mineral, petroleum, and geothermal resources, for studying potential repositories of nuclear waste, and for mapping contaminated groundwater caused by hazardous waste. It is also used in engineering applications, such as mapping the thickness of permafrost.

TEM sounding data are often interpreted in terms of 1-D models because of the computational effort involved in calculating the transient responses of simple 2-D and 3-D structures (*cf.* Adhidjaja, Hohmann & Oristaglio 1985; San Filipo & Hohmann 1985; Newman, Hohmann & Anderson 1986). A layered-earth interpretation of central-loop souding data can be used to map significant electrical boundaries when a small station spacing is used (*cf.* Frischknecht & Raab 1984). However, Frischknecht & Raab (1984)

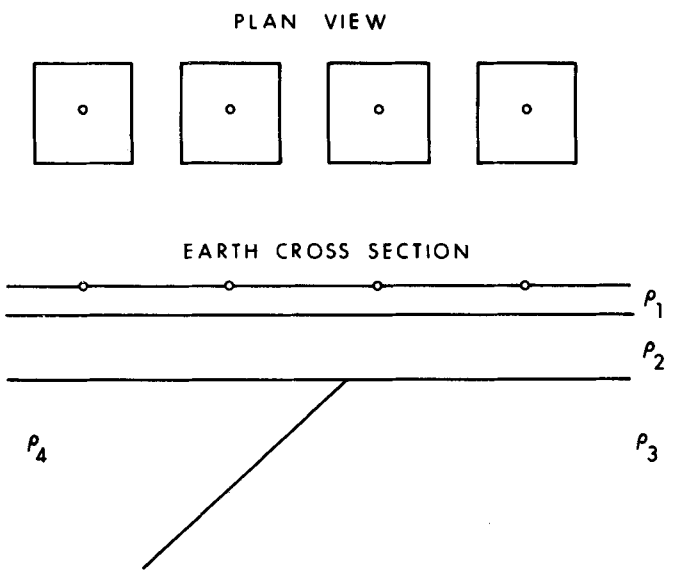

Figure 1. The central-loop sounding method in plan view and earth cross-section. In plan view a transmitter is shown by a square and its receiver by a small circle. The resistivities of the units making up the earth cross-section are depicted by ρ_1, ρ_2, ρ_3, and ρ_4.

conclude that transient soundings distorted by lateral variations in resistivity can be erroneously interpreted with layered-earth models.

In this paper we assess for the first time 1-D model fitting for synthetic data over simple 3-D structures. Our goal is to show when 1-D model fitting is appropriate and when it is not. The horizontal-field measurement made at the centre of the transmitting loop can be an indicator of three-dimensionality because it is theoretically zero if the earth is strictly layered. Therefore, we calculate horizontal fields for a variety of 3-D models and study them as an interpretation tool for mapping and detection of 3-D structures. However, we shall first review 1-D interpretational procedures of central-loop sounding data.

2 One-dimensional interpretation procedures

2.1 INTRODUCTION

In the central-loop sounding method, illustrated in Fig. 1, one usually assumes that the effects of lateral resistivity changes on the measured transient are minimal, and the transient is interpreted as due to a layered earth. A layered-earth model is commonly used to interpret geoelectric measurements because the earth in many cases is approximately horizontally layered, at least locally. Moreover, by compiling localized layered-earth interpretations, more complex 2-D and 3-D structures may be indicated.

The earth is energized by abruptly shutting off the current in the transmitting loop. In response to transmitter shut-off, currents flow in the earth so as to preserve the magnetic field. These currents decay with time and diffuse within the earth. The sensor then measures the magnetic field or the time derivative of the magnetic field (voltage) associated with the decaying current system in the earth.

Nabighian (1979) showed that in the case of a non-polarizable half-space, the system of currents within the earth can be replaced by an equivalent circular filament of current (a 'smoke ring') that expands outward and downward from the transmitter. In the case of a layered earth, Hoversten & Morrison (1982) showed that the pattern of induced electric current is similar. If a conducting layer is present, the current maximum tends to reside within that layer and move mostly laterally away from the transmitter. Eventually, however, the current maximum leaves this layer and diffuses downward, but it is still symmetrical with respect to the transmitter. Because of this current geometry, it is impossible to obtain a sign reversal in a central-loop transient observed over a non-polarizable layered earth.

2.2 FORWARD MODELLING

The forward solution for the vertical magnetic-field transient and its time derivative for a circular loop of radius a on the surface of an n-layered earth can be written in terms of a sine or cosine transform. For a cosine transform, we have

$$h_z(t) = -\frac{2}{\pi}\int_0^\infty \frac{\text{Im}\,[H_z(\omega, \boldsymbol{\rho}, \mathbf{H})]}{\omega}\cos(\omega t)\,d\omega \tag{1}$$

and

$$\frac{\partial h_z}{\partial t}(t) = -\frac{2}{\pi}\int_0^\infty \text{Re}\,[H_z(\omega, \boldsymbol{\rho}, \mathbf{H})]\,\cos(\omega t)\,d\omega, \tag{2}$$

where Re $[H_z(\omega, \boldsymbol{\rho}, \mathbf{H})]$ and Im $[H_z(\omega, \boldsymbol{\rho}, \mathbf{H})]$ are the real and imaginary vertical magnetic-field responses for a layered earth in the frequency domain. The components of the vectors $\boldsymbol{\rho}$ and $\mathbf{H}$ are the resistivities and thicknesses of the layers. Equations (1) and (2) are for a step turn-off in current, where ω is the angular frequency. The complex frequency-domain

response for the vertical magnetic field is given by Ryu, Morrison & Ward (1970),

$$H_z(\omega, \rho, \mathbf{H}) = aI \int_0^\infty \frac{1}{u_0} \left(\frac{Z^1}{Z_0 + Z^1} \right) J_1(\lambda a)\, \lambda^2 \, d\lambda, \tag{3}$$

where $u_i = (\lambda^2 - k_i^2)^{1/2}$ and I is the current in the transmitter. The wave number in the ith layer is given by, $k_i = \sqrt{-j\omega\mu_0/\rho i}$, where $j = \sqrt{-1}$. Note that displacement currents are ignored in the above formulation and that the magnetic permeability is assumed to be μ_0, that of free-space, $4\pi \times 10^{-7}\, H\, m^{-1}$. The input impedance of the ith layer, which is required in equation (3), is given by Wait (1970) as

$$Z^i = Z_i \frac{Z^{i+1} + Z_i \tanh(u_i H_i)}{Z_i + Z^{i+1} \tanh(u_i H_i)}, \tag{4}$$

where the intrinsic impedance of the ith layer, Z_i, is defined as $Z_i = -j\omega\mu_0/u_i$. For the case of the semi-infinite bottom layer, $Z^n = Z_n$. The cosine transforms in (1) and (2) and the Hankel transform in (3) are evaluated using linear digital filtering methods developed by Anderson (1975, 1979).

Since square loops are typically used in practice, the radius of the circular loop in (3) is replaced by $L/\sqrt{\pi}$, where L is the side of the loop. Approximating the area of a square loop to that of a circular loop works well except for the very earliest times.

2.3 APPARENT-RESISTIVITY SOUNDINGS

The data collected from a central-loop sounding usually consist of vertical voltage measurements made at various times after the current is turned off. The voltage measurements are related to the time derivative of the vertical magnetic field in (2) by the relation $V(t) = -\mu_0(\partial h/\partial t)M$, where M is the area-turns product of the receiving coil. Voltage data can be inverted directly for layered-earth models, but voltage curves are difficult to relate directly to the geoelectric section. To aid interpretation, the voltage data are sometimes converted to an apparent-resistivity sounding before inversion. The apparent-resistivity sounding helps define initial estimates of layer resistivities, which are required for non-linear inversion.

The voltage definition of apparent resistivity (ρ_{a_v}) for a step turn-off is obtained by inverting the formula given in Wait (1951),

$$V(t) = \frac{IM\rho}{a^3} \left(3 \operatorname{erf}(\theta a) - \theta a(3 + 2\theta^2 a^2) \frac{2}{\sqrt{\pi}} \exp(-\theta^2 a^2) \right) u(t), \tag{5}$$

for the resistivity, ρ_{a_v}, of a half-space which would reproduce the observed voltage at time t. In equation (5), $u(t)$ is the unit step function and θ is defined by $(\mu_0/4\rho t)^{1/2}$. Following Raab & Frischknecht (1983), we use a reversion of the series to invert (5). As Frischknecht & Raab (1984) point out, the apparent resistivity based on (5) more accurately reflects realistic resistivity values at early times than that calculated using the late-time definition derived from Kaufman (1979),

$$\rho_{a_v} = \frac{\mu_0}{4\pi t} \left(\frac{2\pi a^2 \mu_0\, IM}{5t\, V(t)} \right)^{2/3}. \tag{6}$$

At late times, a calculation based on (5) will give an apparent resistivity that agrees with equation (6).

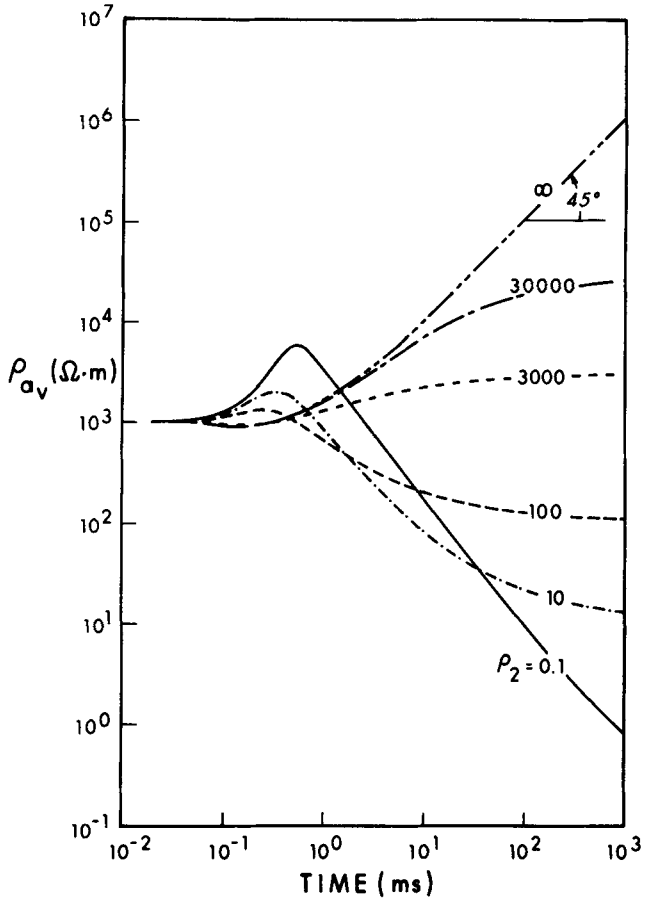

Figure 2. Apparent-resistivity ρ_{a_v} soundings over two-layer earths. The transmitter is a 1200 by 1200 m loop, where the resistivity and thickness of the top layer are 1000 Ω · m and 500 m, respectively. The resistivity of the basal half-space is ρ_2.

Apparent-resistivity soundings for two-layer earths are illustrated in Fig. 2. The top layer is 500 m thick with a resistivity of 1000 Ω · m, and the basement varies from very conductive to insulating. The apparent resistivities, which are based on (5), match the resistivity of the top layer at early times and at late times approach the resistivity of the basal half-space. When the basement is more conductive than the upper layer, the apparent-resistivity sounding shows a characteristic overshoot in apparent resistivity before descending to the lower basement resistivity. In the case of a resistive basement only a slight undershoot in the sounding is observed.

As Raiche (1983) and Spies & Eggers (1986) point out, the overshoot–undershoot problem in the apparent-resistivity sounding can be removed by basing apparent resistivity on the magnetic field, instead of its time derivative. The apparent resistivity ρ_{a_h} can be obtained by using Newton's method (*cf.* Carnahan, Luther & Wilkes 1969) to invert the expression for the vertical magnetic field over a half-space derived in Hohmann & Ward (1987),

$$h_z(t) = \frac{I}{\theta^2 a^3}\left[\left(\frac{\theta^2 a^2}{2} - \frac{3}{4}\right)\operatorname{erf}(\theta a) + \frac{3\theta a}{2\sqrt{\pi}}\exp(-\theta^2 a^2)\right]. \tag{7}$$

Spies & Eggers (1986) show that the apparent resistivity, ρ_{a_v}, as defined by (5) may not even exist in some cases, and in all other cases is multivalued: there exist two exact values of apparent resistivity for each measured voltage. These two values are called early-time and late-time apparent resistivities, because they approach the apparent resistivities given by asymptotic formulas at early and late times. In contrast to the dual valued nature of ρ_{a_v}, there is a one-to-one mapping between ρ_{a_h} and $h_z(t)$.

Several synthetic apparent-resistivity soundings for three-layer earths, based on equations (5) and (7) are shown in Fig. 3(a) and (b). Once again the transmitter is a 1200 by 1200 m square loop. Notice that there are no resistivity overshoots or undershoots in the ρ_{a_h} soundings in Fig. 3(b). Both ρ_{a_v} and ρ_{a_h} soundings show the response of a conductive middle layer to be much more diagnostic than that of a resistive layer. Any inductive sounding method is not nearly as sensitive to resistive layers as it is to conductive layers. Raiche *et al.* (1985) show that a joint inversion of TEM coincident loop and Schlumberger soundings may aid in resolving structures with resistive layers. If a conductive layer is thin with respect to its skin depth, it is well known that an EM sounding is sensitive to the conductance of the layer, but the conductivity and thickness of the layer cannot be resolved independently.

In the case of a two-layer earth with a resistive basement we have never been able to generate an apparent-resistivity sounding in ρ_{a_h} or ρ_{a_v} that rises at an angle greater than 45° on a log–log plot. However, in the case of a very conductive basement or lower layer, the overshoot in the apparent-resistivity sounding as defined by the voltage can rise at an angle

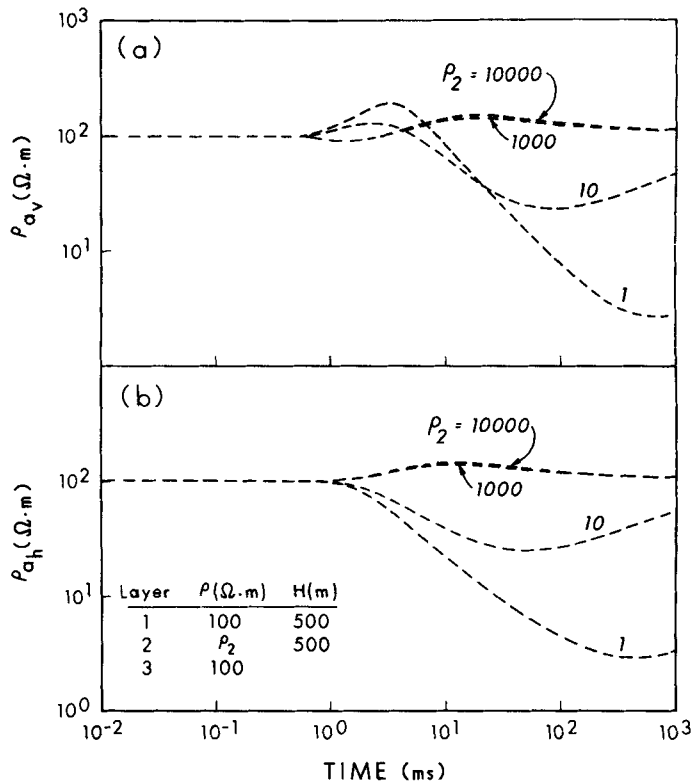

Figure 3. Apparent-resistivity ρ_{a_v} and ρ_{a_h} soundings over three-layer earths. The legend in the lower left-hand corner of the figure shows the resistivities and thicknesses of the layers; (a) and (b).

greater than 45°, as shown by Fig. 2. One may also verify the 45° rise for a two-layer earth where the basement is a perfect insulator by using the late-time voltage formula derived from Kaufman (1979),

$$V(t) = \frac{3IM}{16}\left(\frac{H_1}{\rho_1}\right)^3 \mu_0^4 a^2 t^{-4}, \tag{8}$$

where ρ_1 is the resistivity of the top layer and H_1 is its thickness. By substituting equation (8) into (6), the late-time apparent resistivity, ρ_{a_v}, is defined by

$$\rho_{a_v} = \left(\frac{4}{15}\right)^{2/3} \frac{1}{\mu_0 \pi^{1/3}} \left(\frac{\rho_1}{H_1}\right)^2 t. \tag{9}$$

On a log–log plot of apparent resistivity versus time, equation (9) will plot as a straight line with a slope of 1 and the apparent resistivity will exhibit a 45° rise with increasing time. One can follow a similar derivation for the late-time, magnetic-field definition of apparent resistivity.

2.4 INVERSION

Two approaches exist for solving the TEM non-linear inverse problem. The first is to make no assumption on the conductivity distribution in the Earth and find the classes of conductivity models that fit the data. The second, which is more practical in many exploration problems, is to assume a model that is supposed to represent that part of the Earth under consideration. The parameters of the model are then estimated using an optimization technique.

An essential aspect of this second approach, which is called model fitting, is the assumption of the correct class of model; layered earth, dike, cylinder, etc. Model fitting allows for geological and geophysical information to be incorporated into the inverse problem, in the form of constraints, and thereby alleviates some of the non-uniqueness problems. The disadvantage of model fitting is that the Earth is always more complex than the assumed model and an unknown bias is introduced into the inverse problem (Draper & Smith 1981).

For the inverse problem we will use the model-fitting approach, where the model is a layered earth with parameters consisting of layer resistivities and thicknesses, and investigate the bias introduced by lateral resistivity changes. A classical technique for solving a parameter estimation problem is the method of least-squares. In order to obtain an inverse solution, an iterative linearization method is often used, such as the Levenberg–Marquardt method (*cf.* Inman 1975; Leite & Leão 1985). The Levenberg–Marquardt method is a modified least-squares solution, where small eigenvalues in the sensitivity matrix are damped out. Inman (1975) used this method for layered-earth inversions of Schlumberger sounding data.

Since a realistic layered-earth inverse solution will be sought, a constrained optimization algorithm is advised. Anderson (1982) modified a general non-linear least-squares algorithm of Dennis, Gay & Welsch (1981) to that of a constrained or unconstrained algorithm with weighted observations. The algorithm of Dennis *et al.* (1981) maintains a secant approximation to the second order least-squares Hessian and is more reliable than a Gauss–Newton or Levenberg–Marquardt algorithm when a large residual exists between the data and the forward solution.

The inversion program NLSTCI (Anderson 1982), based on the Dennis *et al.* (1981) algorithm, computes the transient forward solution defined by (1)–(3). The forward solution is constructed in the frequency domain and then it is Fourier transformed to the time domain. Program NLSTCI allows for central-loop inversions to be carried out with magnetic-field, voltage or apparent-resistivity data. Converting magnetic-field or voltage data to apparent resistivities reduces the dynamic range of the data, but does not improve the final layered-earth estimates.

An important problem in any inverse solution is estimating parameter resolution and accuracy. For many transient soundings there will be a class of layered-earth models that fit the data at an acceptable level. One approach for assessing the solution is to assume that in the region of parameter space about the solution the data can be described approximately by linear functionals of the parameters. Linear statistical methods then can be used for assessing the solution (*cf.* Inman 1975). However, Bard (1974) and Inman (1975) point out that linear statistical properties of solutions derived from highly non-linear inverse problems can be meaningless and misleading. Nevertheless we will use linear statistics; the uncertainties in the estimated parameters will be given in terms of standard errors and when a large correlation between two respective parameters occurs, the correlation will be noted. When two parameters are highly correlated, standard error estimates of the respective parameters may be meaningless.

We also realize that linear statistics tell us nothing about inverse solutions at other minima. An empirical way of assessing inverse solutions at other minima is to test the sensitivity of a solution to its initial guess, an approach that we will apply. Because we are primarily interested in an assessment of the bias involved in fitting layered earths to data obtained over 3-D structures, no random noise will be added to the synthetic data.

3 Interpretation of synthetic soundings over a 3-D conductive structure

3.1 FORWARD MODELLING

The TEM response for a simple 3-D structure must first be understood before discussing an interpretation of the structure based on layered-earth models. The 3-D soundings presented in this paper are calculated using a frequency-domain integral equation solution and subsequently are Fourier transformed to the time domain (refer to Newman *et al.* 1986 for details). The Fourier transform is carried out using the imaginary part of the 3-D frequency response. The imaginary part is preferred because it has greater accuracy than the real part at lower frequencies for loop sources. Thus (1) is used for the magnetic field. However, the time derivative of the field is not evaluated with (2) but rather with a sine transform,

$$\frac{\partial h}{\partial t}(t) = \frac{2}{\pi} \int_0^\infty \text{Im}\,[H(\omega)]\, \sin(\omega t)\, d\omega. \tag{10}$$

At late times we differentiate the magnetic-field transient in (1) to obtain the time derivative of the field. The magnetic-field transient is replaced with a cubic spline and the spline is differentiated to obtain $\partial h/\partial t$. Evaluating $\partial h/\partial t$ in this manner does not amplify numerical noise and is more accurate than evaluating equation (10) directly at late times. The accuracy problem is explained by the dynamic range of the calculations needed to evaluate (10); the dynamic range of the calculations needed for the magnetic field is less, hence the magnetic field is more accurate. Calculating a 3-D transient sounding typically requires 20–40 frequency-domain evaluations, over a sufficiently wide band width. The sampling rate is typically 5–8 points per decade of frequency.

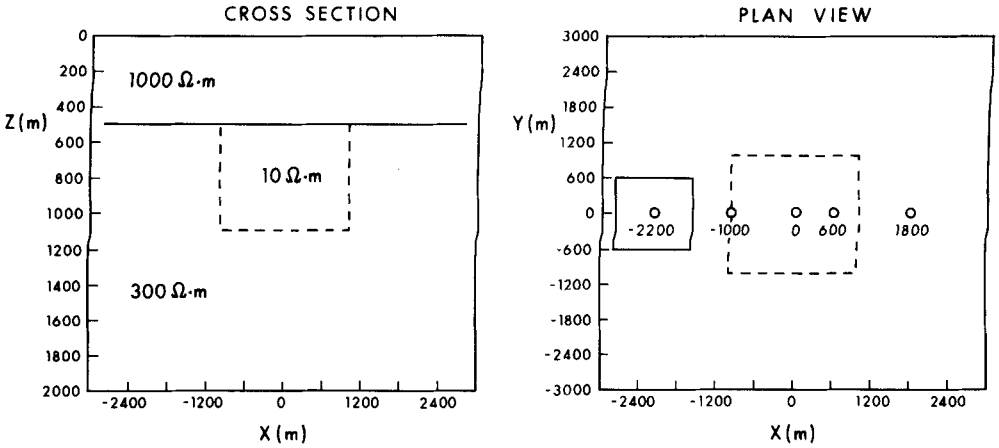

Figure 4. 3-D conductive body in a two-layer earth. The model is typical of a geothermal exploration target. The body is outlined by the dashed lines. The transmitting loop is only shown at −2200. Central-loop soundings are calculated at −2200, −1000, 0, 600 and 1800.

Fig. 4 shows a 3-D model of a conductive body taken in part from a model catalogue of Anderson & Newman (1985). The 10 Ω · m conductor represents a conductive hot water zone, typical of a geothermal exploration target. The two-layer host consists of 1000 and 300 Ω · m material; the thickness of the top layer is 500 m. The 3-D conductor has dimensions 2000 by 2000 m in the horizontal directions and a thickness of 600 m. The body is buried at a depth of 500 m. Central-loop soundings are calculated on a profile over the conductor at $x = -2200$, -1000, 0, 600 and 1800; the transmitter is a 1200 by 1200 m square loop.

At station 600, for example, as shown in Fig. 5, the 3-D apparent-resistivity responses,

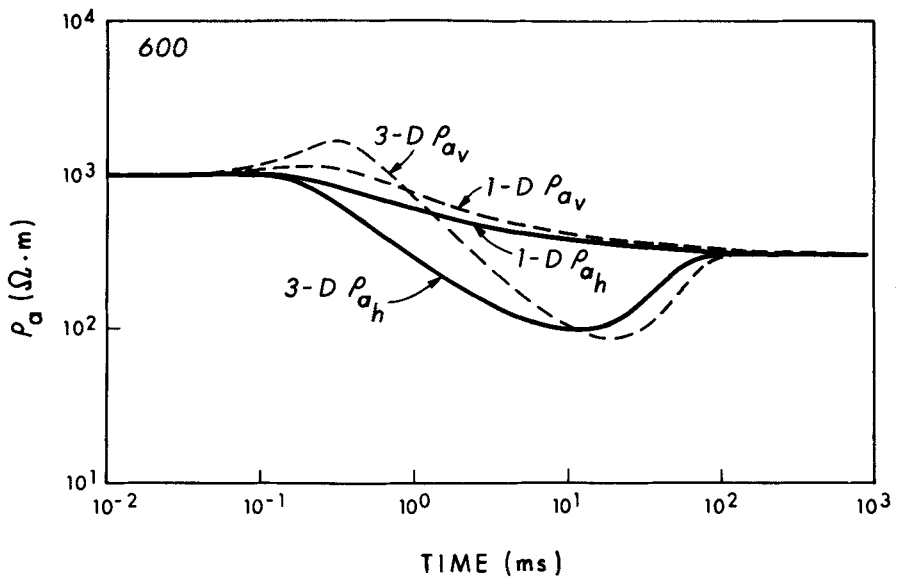

Figure 5. 3-D apparent-resistivity (ρ_{a_h} and ρ_{a_v}) responses at station 600. The 1-D responses are shown for comparison. The dashed curves are the ρ_{a_v} soundings, while the solid curves are the ρ_{a_h} soundings.

ρ_{a_h} and ρ_{a_v} are band limited, and are not distinguishable from the 1-D soundings at early and late times. Note that the 1-D soundings are defined by the layered earth only. The 3-D ρ_{a_v} sounding shows an overshoot in apparent resistivity before dipping below the 1-D ρ_{a_v} sounding. However, this apparent-resistivity overshoot is not strictly a 3-D effect, because layered-earth ρ_{a_v} soundings show the same thing (*cf.* Figs 2 and 3a).

3.2 LAYERED-EARTH MODEL FITTING

The data fits and the interpreted models in Figs 6 and 7 are based on inversions using the magnetic-field definition of apparent resistivity. The data fit for station −2200 is not shown in Fig. 6, because it is similar to that at station 1800. The minimum number of layers required for an acceptable data fit was four; adding additional layers did not reduce significantly the final rms (root mean square) error. The top layer and basal half-space resistivities were constrained at 1000 and 300 Ω · m for the interpretation shown in Fig. 7. A constrained interpretation is justified because the observed soundings reflect 1000 and 300 Ω · m material at early and late times.

At stations 0 and 600 we could not find a layered-earth model that fits the data very well, in particular between 10 and 200 ms (Fig. 6). The observed soundings at these two stations change too rapidly with time to be matched with a realistic layered-earth model. We know from 1-D forward modelling that an insulating basement could cause a 1-D sounding to rise just as steeply as the observed soundings do between 20 and 100 ms. However, such an interpretation would not fit the data after 100 ms.

The interpreted section in Fig. 7, based on the results in Fig. 6, show that the 3-D body has been indicated by the second conductive layer and the third resistive layer. The

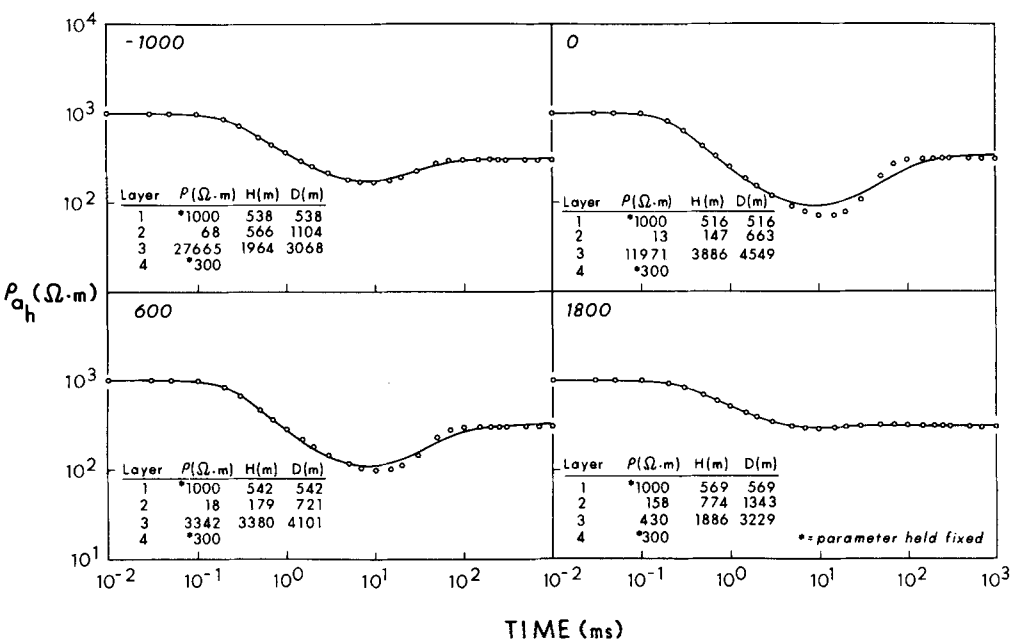

Figure 6. Layered-earth fits to the ρ_{a_h} data calculated from the 3-D model in Fig. 4. The open circles are the synthetic data and the solid lines are the layered-earth fits. The figure legends show the least-squares solutions and the parameters held fixed are denoted with an '*'.

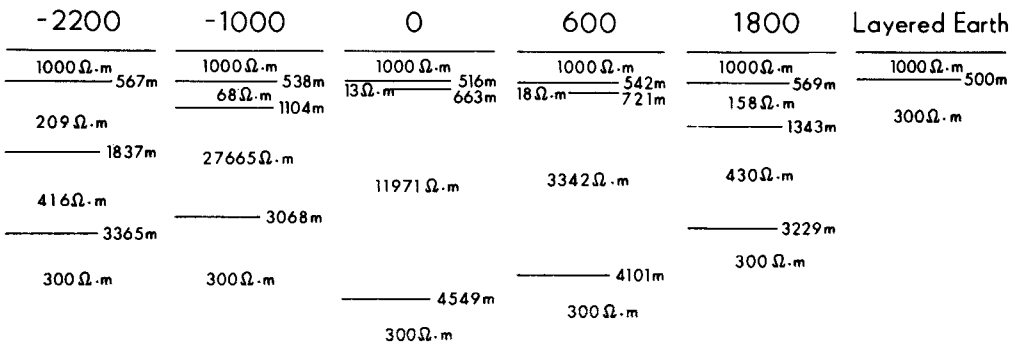

Figure 7. Interpreted ρ_{a_h} section for the 3-D model in Fig. 4.

conductive and resistive layers relate to the 3-D sounding dropping below and subsequently rising back to the 1-D sounding curve at early and late times (Fig. 5). The conductive layer below the top 1000 Ω m^{-1} layer is naturally most conductive for stations at –1000, 0 and 600. However, it becomes less conspicuous away from the conductor at –2200 and 1800. The resistivities of the layer range from 13 to 209 Ω m^{-1} and appear to be highly correlated with the thickness of the layer. Correlations as high as –0.99 are typical for the conductivities and thickness of this layer, over the conductor. In essence the conductance of the second layer underestimates the conductivity-thickness product of the 3-D structure. As expected, the high resistivity values of the third layer over the conductor are not very well resolved; errors in the estimated resistivities range from 22 to 40 per cent. However, the corresponding thickness estimates of the layer appear to be better resolved; the errors are less than 9 per cent. The interpreted depths to the second layer are also well resolved; in Fig. 7 the estimated depths to the layer vary between 516 and 567 m and the errors are less than 3 per cent. These percentage errors given above are defined by the standard error of an estimated parameter divided by the estimate.

An interpretation using the voltage definition of apparent resistivity showed a section very similar to that in Fig. 7. Once again the minimum number of layers required for an acceptable data fit was four and the data fits at stations 0 and 600 were not very good between 10 and 200 ms. For the model in Fig. 4, we find no advantage in using an interpretation that is based on the magnetic field or its apparent resistivity.

At stations 0 and 600, truncating the data at 20 ms allows for improved layered-earth fits. Fig. 8 shows such an example of a layered-earth fit to a truncated ρ_{a_v} data set (station 0). Two layers are used in the interpretation, because the truncated sounding indicates two layers. The resistivity of the top layer is based on the early-time apparent resistivity in Fig. 8 and is constrained at 1000 $\Omega \cdot$ m. The solution for the thickness of the top layer and the basal half-space resistivity is found to be quite stable by starting the inversion at different resistivities and thicknesses and obtaining the same final solution. Moreover, error estimates for the layer thickness and basal half-space resistivity are less than 2 per cent for the solution shown in Fig. 8. From Fig. 8, we suggest that a two-layer interpretation will give an accurate estimate of the depth to the conductor, but an overestimate of the conductor's resistivity.

Synthetic 3-D data may reproduce characteristics of field data that are difficult to interpret with layered-earth models. The ρ_{a_v} sounding in Fig. 9(a), is an example of such a case. This sounding was obtained from a survey conducted over the Medicine Lake geothermal area in northern California (Anderson *et al.* 1983). Beyond 10 ms the sounding

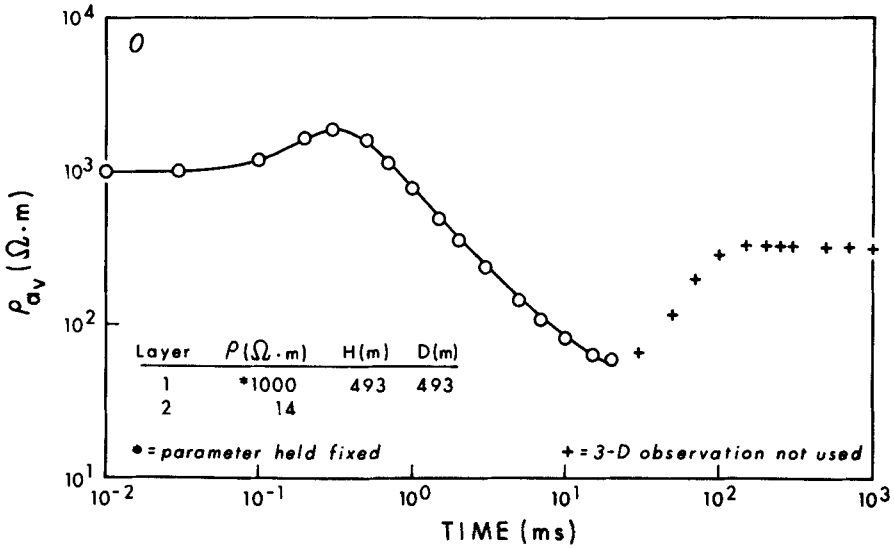

Figure 8. An example of 1-D model fitting to a truncated ρ_{a_v} data set at station 0, in Fig. 4. The plus signs are the 3-D observations not used in the interpretation. The legend in the lower left-hand corner of the figure is the interpreted model.

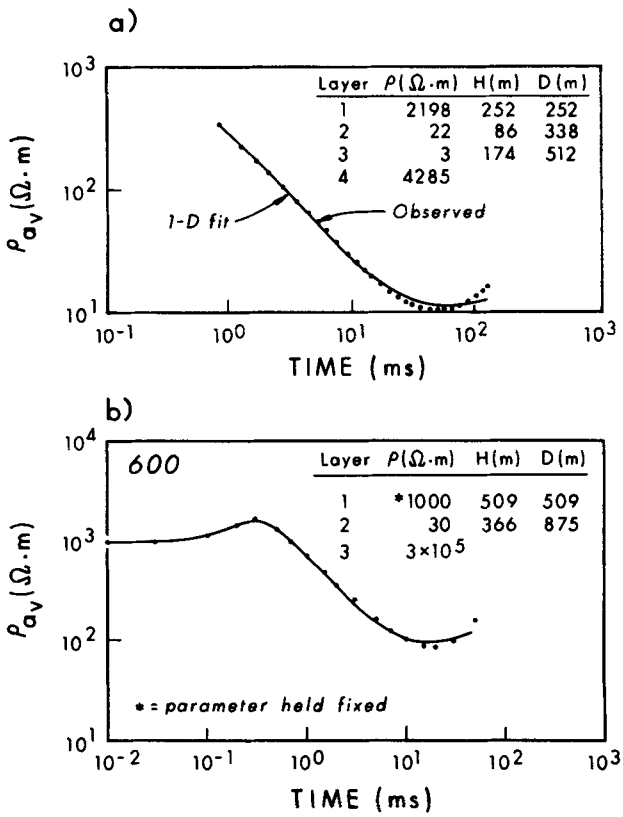

Figure 9. Field data and 3-D synthetic data that are difficult to interpret with layered-earth models. The field data in (a) are from the Medicine Lake geothermal area and the synthetic data in (b) are from the geothermal model of Fig. 4.

changes too rapidly with time for a reasonable layered-earth interpretation. An apparent-resistivity overshoot due to a very thick conductive lower layer can be used to fit the data after 10 ms, but the interpreted model is meaningless. Fig. 9(b) shows the ρ_{a_y} synthetic sounding for the geothermal model of Fig. 4 at station 600, and an attempted layered-earth fit, where the data are truncated beyond 50 ms. Note the striking similarity between the field data and the synthetic data and the corresponding data fits after 10 ms. We conclude that interpreting the Medicine Lake data in Fig. 9(a) with layered-earth models is not appropriate. The interpretation of the data must be based on 2-D or 3-D models.

3.3 HORIZONTAL-FIELD INTERPRETATION

In theory, the horizontal-field measurement can be used to map and detect 2-D or 3-D structure in a layered earth, because the response of any layered earth is zero. Horizontal magnetic-field and voltage calculations for the model of Fig. 4 are shown in Fig. 10. The calculations are made at the centres of the transmitting loops; hence there is no layered-earth response.

The magnetic-field and voltage calculations in Fig. 10 show that the horizontal responses on the left side of the conductor (−2200 and −1000) are opposite in sign to the responses on the right side of the conductor (600 and 1800). When transmitters are located on the right side of the conductor, the direction of the electric currents flowing through the conductor reverses with respect to the transmitters located on the left at −2200 and −1000. Therefore, there is a corresponding reversal in the sign of the magnetic field and voltage. The horizontal responses in Fig. 10 are dominantly galvanic for stations other than at 0 because

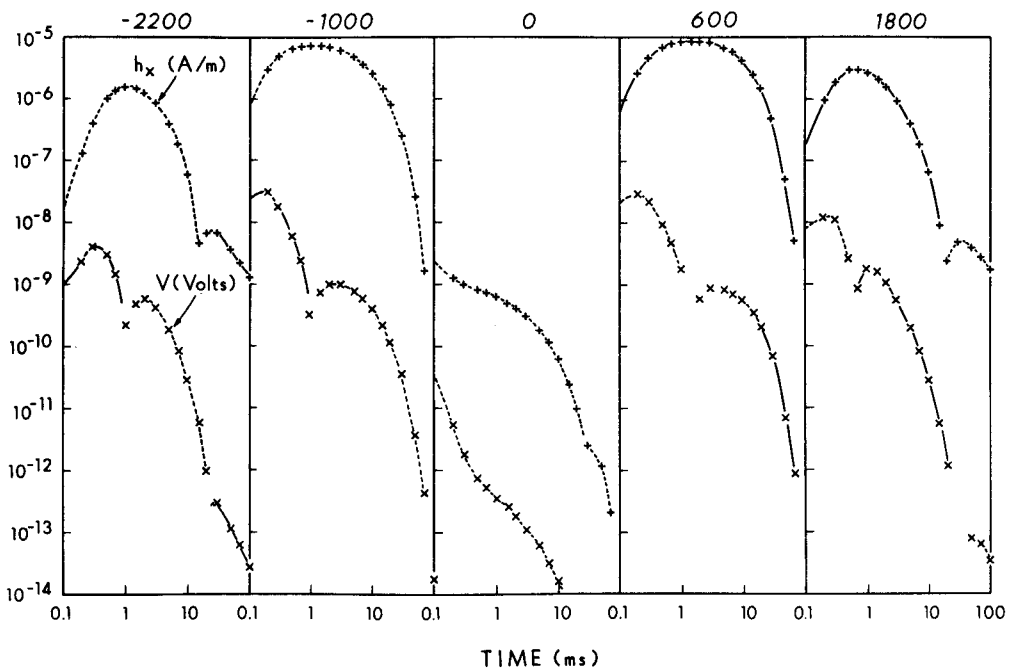

Figure 10. Horizontal magnetic-field and voltage responses (h_x and V_x). Solid curves define positive responses and dashed curves define negative responses. The magnetic field responses are depicted by plus signs and the voltage responses by crosses.

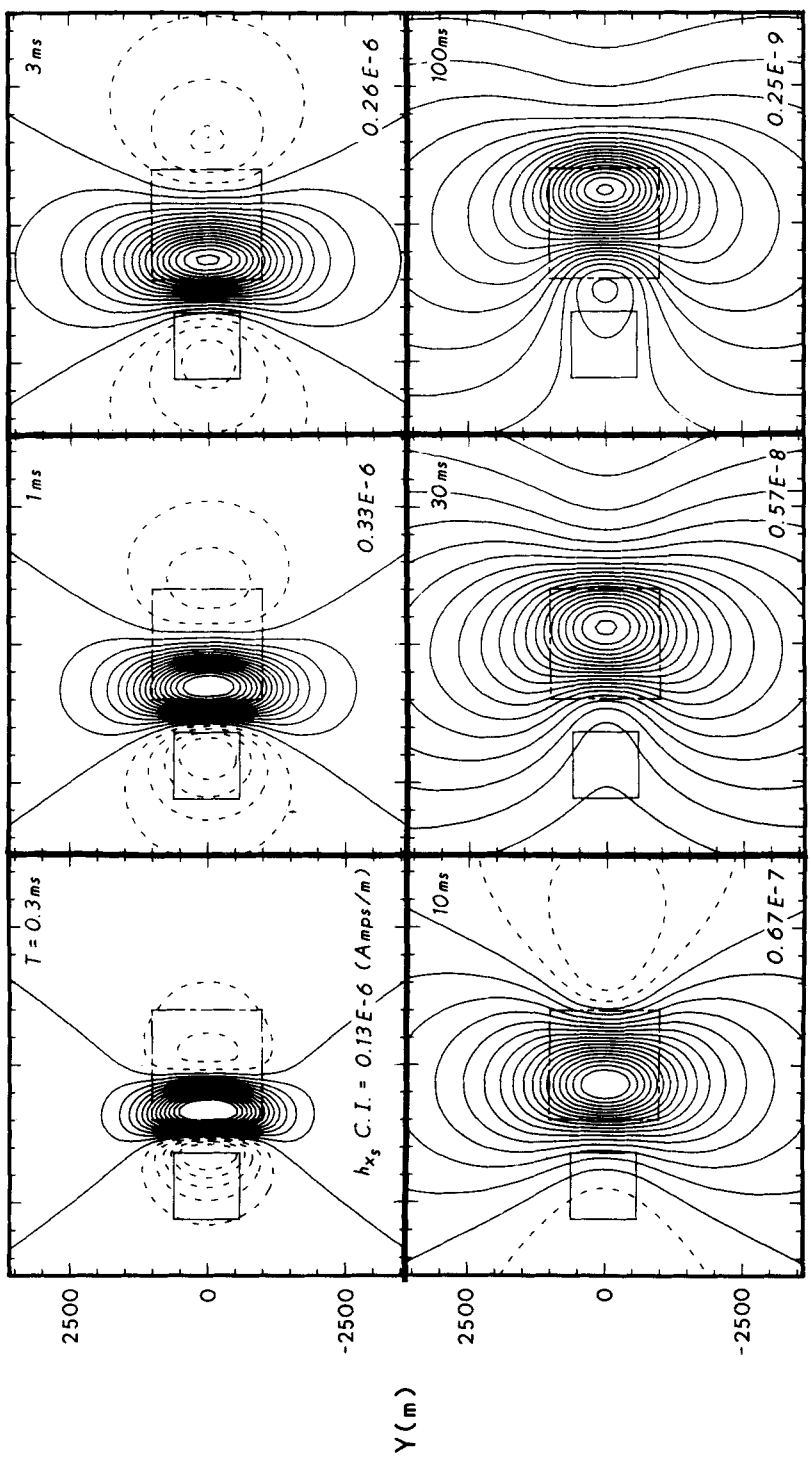

Figure 11. Time slice maps of the horizontal scattered magnetic field (h_x) at 0.3, 1.3, 10, 30 and 100 ms. The transmitter is the small square and is centred at −2200. The surface projection of the 3-D body is shown as the large square. The contour interval is given at the bottom of each time slice map. Dashed contours correspond to negative field values. In each plot, y is positive upward and x is positive to the right.

the contrast in conductivity between the body and host is only 30 to 1 (Newman *et al.* 1986). At station 0, the horizontal response are several orders of magnitude smaller than at the other stations, because the transmitting loop is positioned directly over the conductor's centre.

The sign reversals in both magnetic field and voltage in Fig. 10 can be explained by inspecting spatial plan maps of the horizontal magnetic field scattered by the conductor at various times. The magnetic field at a particular time is directly related to the existing currents in the earth by the Biot–Savart law (Nabighian 1982). The voltage response on the other hand is related to the time derivative of these currents and is more complicated to interpret.

Fig. 11 shows time-slice maps of the scattered horizontal magnetic field at six times at the surface of the earth with the transmitting loop centred at −2200. The scattered field is defined by the difference between the total and layered-earth fields. Between 0.3 ms and 10 ms, the magnetic-field response of the conductor shows a negative field pattern adjacent to the conductor, but a positive field pattern over the left side of the conductor. The positive field pattern is caused by currents that are channelling through the conductor, and the negative field pattern is caused by the corresponding return currents. By 30 ms, the negative field pattern has moved beyond the boundaries of the time-slice maps, and the field is positive in the displayed area, everywhere.

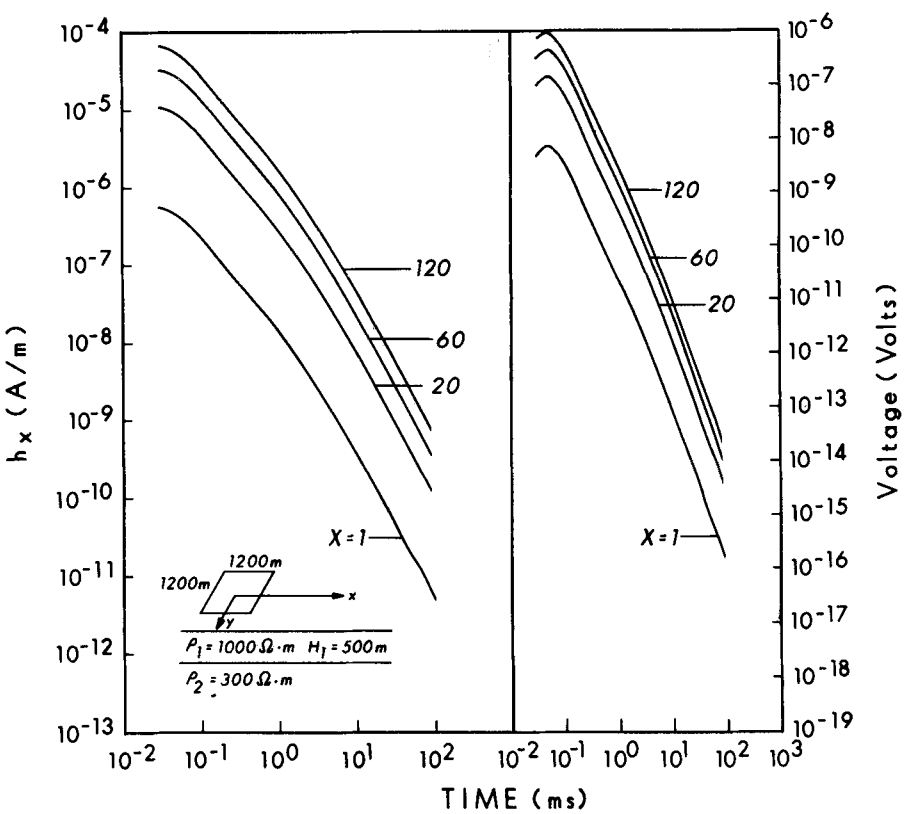

Figure 12. Layered-earth horizontal magnetic-field and voltage responses. The sensors are located along the x-axis from 1 to 120 m away from the centre of the transmitter. The layered-earth model and transmitter are shown in the lower left-hand side of the figure.

We can now explain the magnetic-field and voltage sign reversals in Fig. 10. The peak magnetic-field response at 1 ms at station −2200 corresponds to the time when channelled and return currents are maximized about the conductor (inspect the amplitudes of the contour intervals in Fig. 11). Hence, there is a corresponding reversal in the voltage at this time. The sign reversal in the magnetic field at 15 ms is explained by the negative field pattern (in Fig. 11) moving out from the conductor and past the centre of the transmitter between 10 and 30 ms. The sign reversal in the voltage after 15 ms is caused by a local peak in the magnetic field after its sign change at 15 ms. Soundings at other stations exhibit similar behaviour, but with varying degree. The magnetic-field sign reversals at stations −1000, 600 and 1800 occur later in time. Note also that the magnetic-field sign reversals at stations −1000 and 600 also occur after 100 ms.

In practice the horizontal-field response of the layered earth can never be made zero, because it is sensitive to sensor placement and noise. A sensor that is not positioned accurately at the centre of the transmitter could produce significant layered-earth response. Fig. 12 shows the sensitivity of the layered-earth magnetic-field and voltage responses to position; sensors are placed from 1 to 120 m away from the centre of the transmitter, along the x-axis. If the calculations were made from −1 to −120 m, there would be a corresponding reversal in the sign of the 1-D responses when compared with Fig. 12. It is very important to note the magnitude of the layered-earth response before drawing any conclusions concerning the detectability of 3-D structures with horizontal-field measurements.

When a sensor is misplaced 120 m from the centre of the loop (Fig. 12), the horizontal-field interpretation of the conductor with magnetic-field and voltage measurements (Fig. 10) will be affected out to about 1 ms; a sensor placed at 120 m corresponds to a position that is 18 per cent of the radius of the transmitter. After 5 ms, the response of the conductor at stations −1000 and 600 is so large compared with the layered-earth response that placement of the sensor is not so important. The above analysis does not include the effect of natural electromagnetic noise, which will certainly make the horizontal-field measurement more difficult to interpret.

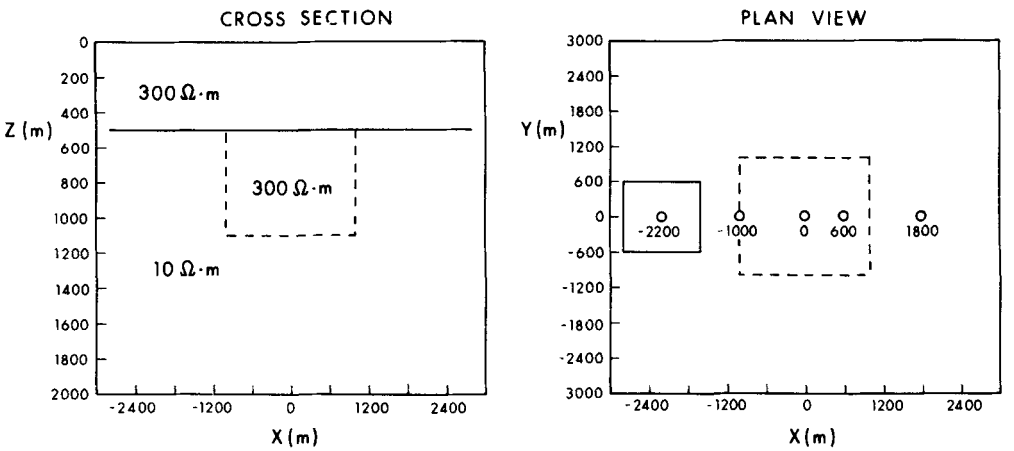

Figure 13. Variable-depth, resistive, overburden model. The model represents a buried river channel. The 3-D structure is illustrated by dashed lines.

4 Interpretation of synthetic soundings over a 3-D resistive structure

4.1 FORWARD MODELLING

The 300 Ω · m resistive body in Fig. 13 is an overburden structure model, where depth to 10 Ω · m conductive basement varies. The structure could be representative of a buried river channel. The 3-D model in Fig. 13 is identical in spatial geometry to the geothermal model in Fig. 4 and is also taken in part from Anderson & Newman (1985). Once again the central loop soundings are calculated at $x = -2200$, -1000, 0, 600 and 1800, where the transmitting loops are 1200 m on a side.

The 3-D apparent-resistivity responses in Fig. 14 are band limited, where the response of the 3-D body vanishes at early and late times. This behaviour indicates that basement resistivity can be recovered when the data are inverted. Note that the 3-D ρ_{a_v} sounding in Fig. 14 shows a resistivity undershoot between 0.5 ms and 3 ms, in contrast to the 1-D ρ_{a_v} sounding. Once again the resistivity undershoot in ρ_{a_v} is not strictly a 3-D effect because a ρ_{a_v} layered-earth sounding can also exhibit it. As time progresses both 3-D soundings rise above the corresponding 1-D soundings.

4.2 LAYERED-EARTH MODEL FITTING

Layered-earth data fits and an interpreted section of the overburden model in Fig. 13 are shown in Figs 15 and 16, respectively. The data are defined by the magnetic-field definition of apparent resistivity and three layers are required for an acceptable data fit. The response of the 3-D structure is so weak at stations −2200 and 1800 that the data show only the layered-earth response of Fig. 13. However, at stations −1000, 0 and 600 a change in the thickness of the overburden is quite obvious, as shown by the interpretation in Fig. 16.

Beneath the constrained 300 Ω m^{-1} layer, the interpreted section shows a pattern of

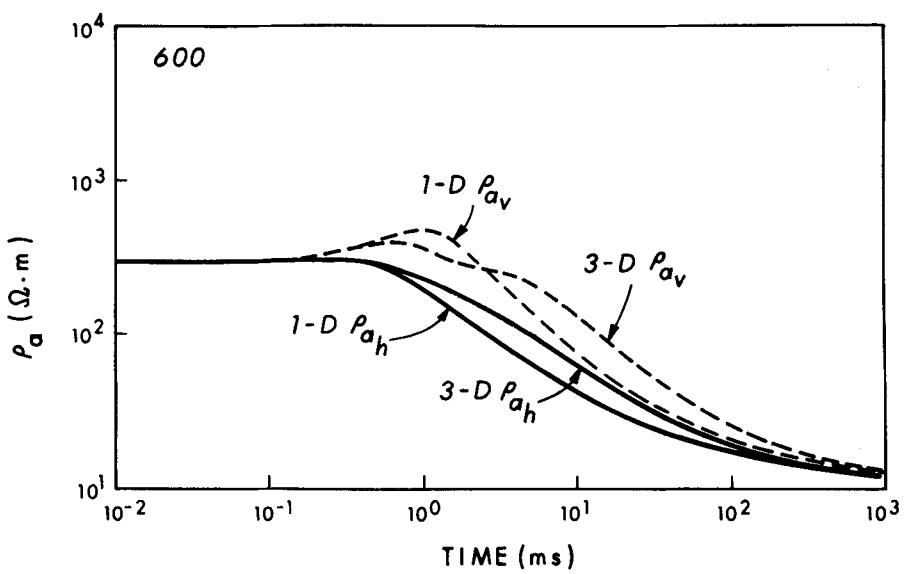

Figure 14. 3-D and 1-D apparent-resistivity responses at station 600 for the overburden model of Fig. 13. The 1-D responses are for the background layering. Solid curves are the ρ_{a_h} soundings and the dashed curves are the ρ_{a_v} soundings.

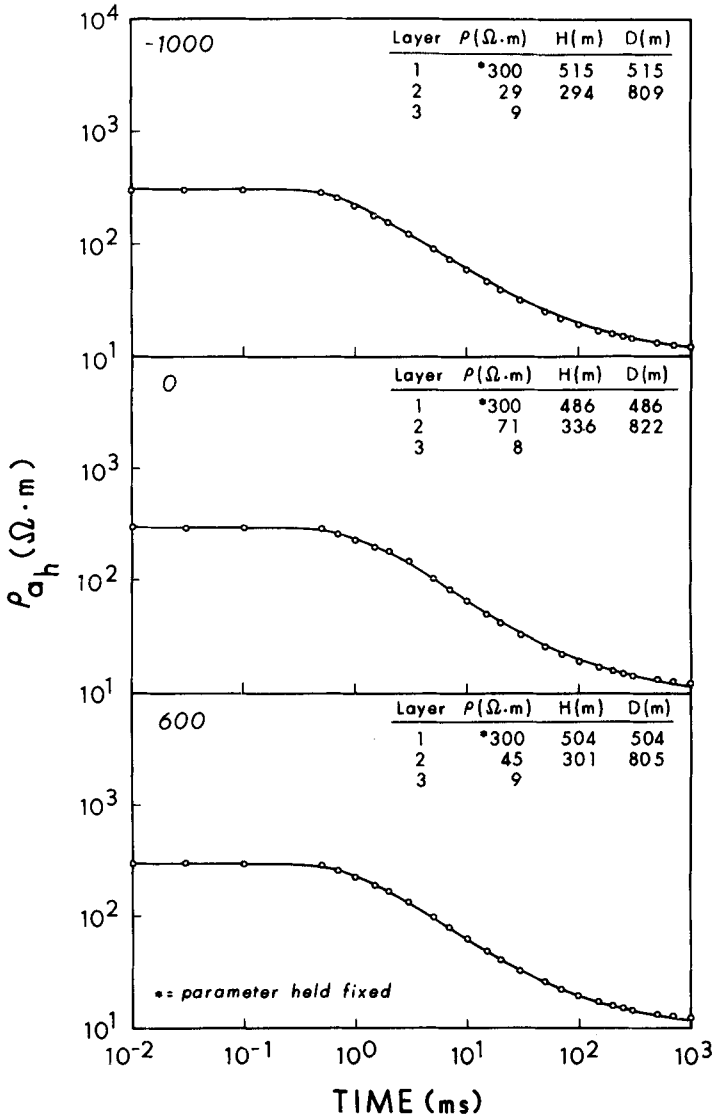

Figure 15. Layered-earth fits to the ρ_{a_h} data for the model of Fig. 13. The open circles are the data and the solid lines the data fits.

resistivity decreasing with depth to conductive basement (Fig. 16). The estimates of the resistivity of the basement are very close to the correct value of $10\,\Omega \cdot$ m; the errors in the basement resistivities are less than 2 per cent. The resistivities of the second layer are 29, 71 and $45\,\Omega \cdot$ m at stations -1000, 0 and 600, respectively. This layer shows the increase in the thickness of the overburden. The resistivity and thickness of the second layer is well resolved; the errors range from 4 per cent to 8 per cent for the resistivities while the errors in the thicknesses are less than 3 per cent. The depths estimated to the second layer vary from a minimum to 486 m at station 0 to a maximum of 515 m at station -1000 and they are also well resolved; the errors are less than 3 per cent.

Figs 17 and 18 show layered-earth data fits and an interpreted section of the overburden

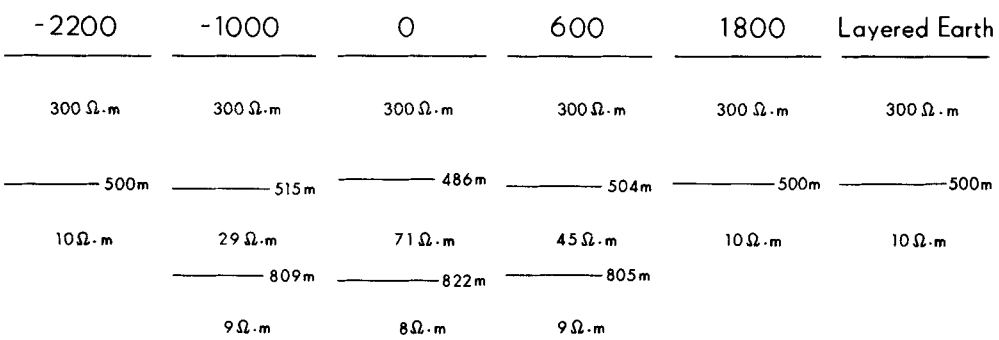

Figure 16. Interpreted ρ_{a_h} section for the model of Fig. 13. The data at stations −2200 and 1800 show only the background layered-earth.

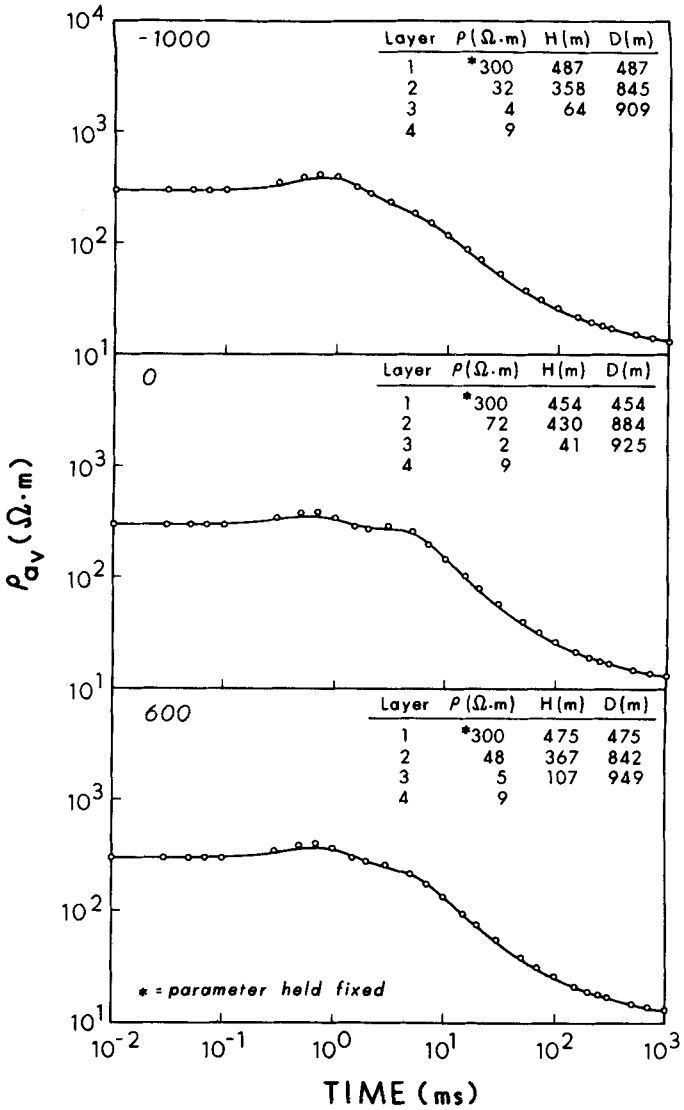

Figure 17. Layered-earth fits to the ρ_{a_v} data for the model of Fig. 13.

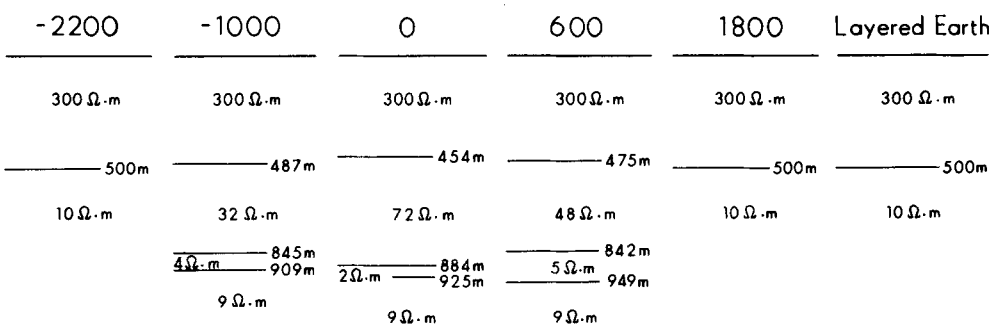

Figure 18. Interpreted ρ_{a_v} section for the model of Fig. 13.

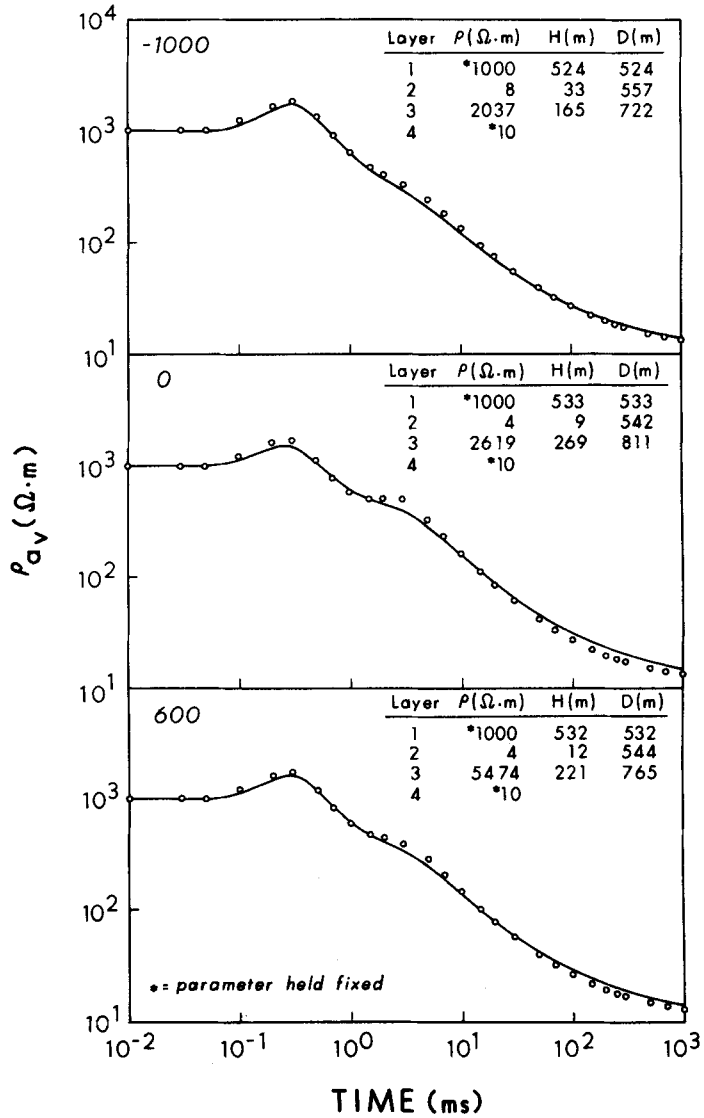

Figure 19. Layered-earth fits to ρ_{a_v} data. The ρ_{a_v} data are calculated for the model of Fig. 13, with the resistivity of the overburden increased to 1000 Ω m^{-1}.

model using the voltage definition of apparent resistivity. Overall the interpreted sections in Figs 16 and 18 are quite similar. The most important difference is the number of layers required for an acceptable data fit; four layers were needed to interpret the ρ_{a_v} data, while only three were required for the ρ_{a_h} data. The thin conductive third layer in Fig. 18 is essential if acceptable data fits are to be achieved at late times (> 100 ms). We do not have a good physical explanation of the need for a third layer; however, it may be required because the 3-D ρ_{a_v} response appears to last longer in time than the 3-D ρ_{a_h} response (Fig. 14). The important aspects of the ρ_{a_v} interpretation are the thickness of the top layer, the resistivity and thickness of the second layer and the basement resistivity. These layered-earth estimates are well resolved since their errors are very close to the errors quoted in the ρ_{a_h} interpretation.

Increasing the resistivity of the overburden in Fig. 13 to 1000 Ω · m has a drastic effect upon a layered-earth interpretation that is based on voltage data. A very strong resistivity undershoot is observed in the data between 0.3 ms and 1 ms (Fig. 19); the undershoot is more clearly emphasized once the 3-D responses are compared with the background layered-earth response as in Fig. 14. This resistivity undershoot in Fig. 19 is interpreted as due to a thin conductive layer beneath the top 1000 Ω · m layer, as shown in Fig. 20. The undershoot is so strong at station 0 that it is difficult to fit the data to a layered-earth model between 2 and 5 ms. Note that this time range is after the observed undershoot; fitting the undershoot has resulted in a poorer fit to the data at later times. The conductivities and thicknesses of the thin second layer are highly correlated in a negative sense, correlations of –0.98 are typical. Beneath the thin conductive layer, the third layer shows a poorly resolved zone of high resistivity; errors for the estimated resistivities range between 50 and 60 per cent. However, the thicknesses of the third layer are well resolved; the errors are around 6 per cent. We were forced to constrain the basement resistivity if four layers were to be used to fit the data. Additional layers did not improve the data fits shown in Fig. 19.

We point out that transforming voltage data to apparent resistivity did not introduce ambiguities into the interpretation illustrated in Figs 19 and 20. When inversions are carried out using voltage, the interpreted section is nearly identical to that shown in Fig. 20.

The thin conductive layer and the deeper resistive layer are indications that there is an increase in the thickness of the 1000 Ω · m overburden. Unlike the ρ_{a_h} and ρ_{a_v} interpretations for the 300 Ω · m overburden, the interpretation of data for the 1000 Ω · m overburden is drastically different: estimates of the resistivity and thickness of the second layer and the resistivity of the third layer are poorly resolved and not realistic. Removing

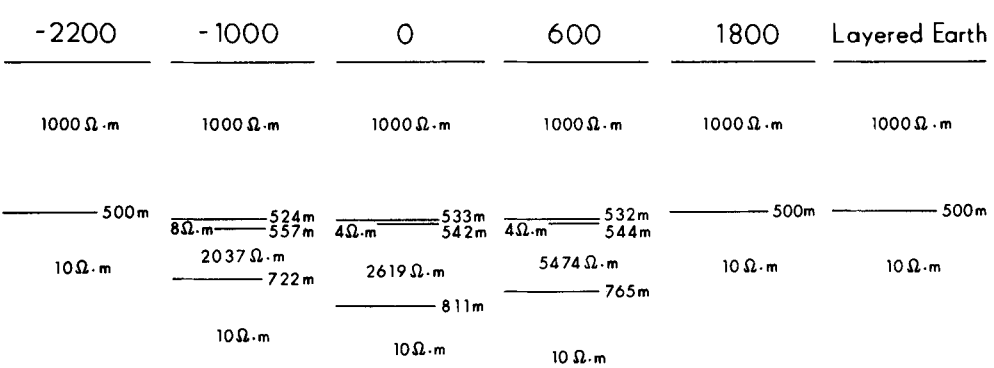

Figure 20. Interpreted ρ_{a_v} section for the data of Fig. 19. The data at stations –2200 and 1800 show only the background layered-earth response.

the resistivity undershoots in the data in Fig. 19 is essential for an improved interpretation. These undershoots caused the addition of the misleading thin conductive layer and resulted in poor estimates on the resistivity of the third layer in Fig. 20.

In the case of the 1000 Ω · m overburden model, Figs 21 and 22 show that a ρ_{a_h} interpretation is superior. Because no resistivity undershoots are present in the data, fewer layers are required in the interpretation, and much better data fits are achieved (compare Fig. 19 to Fig. 21). The interpreted section in Fig. 22 is similar to those in Figs 16 and 18. The errors in the resistivities of the second layer range from 4 to 6 per cent and corresponding thicknesses range from 3 to 5 per cent. The basement resistivities are also well resolved; their errors are less than 4 per cent. Once again, if the data were the magnetic field instead of

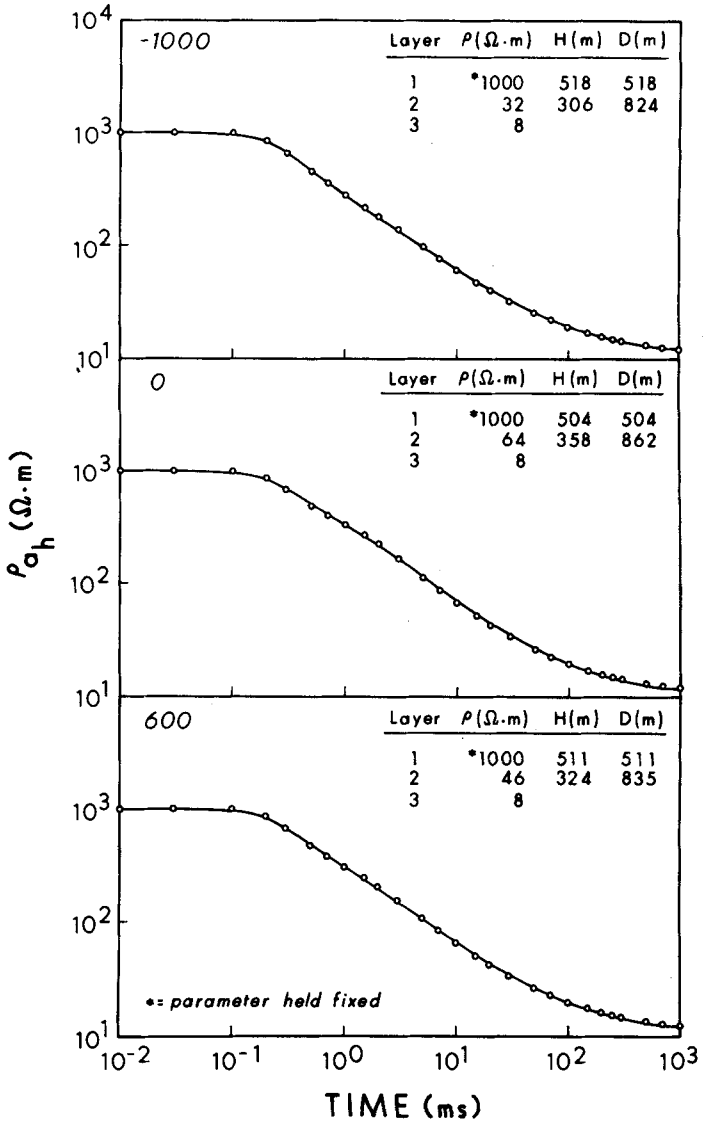

Figure 21. Layered-earth fits to ρ_{a_h} data for the model of Fig. 13, with the resistivity of the overburden increased to 1000 Ω · m.

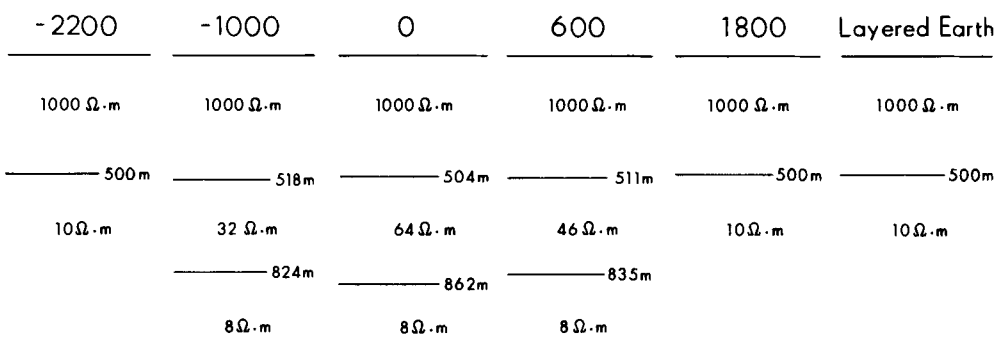

Figure 22. Interpreted ρ_{a_h} section for the data of Fig. 21.

apparent resistivity, inversion of the data gives nearly identical interpretations as shown in Figs 21 and 22.

The differences in the interpretations of Figs 20 and 22 are not surprising to us. When data are from layered earths we expect the interpretations based on the magnetic field and voltage be identical. However, we have no reason to expect this when the data are from 3-D earths.

Fitting layered-earth models to a 300 or 1000 Ω · m variable-depth overburden underestimates its thickness. The maximum thickness of the overburden is 1100 m; in all interpreted cases (ρ_{a_h} and ρ_{a_v}), the maximum depth estimated to basement is less than 950 m. It also appears from Figs 16, 18, 20 and 22 that 1-D model fitting will estimate well the depth at which the overburden begins to increase in thickness, 500 m; in all interpreted cases, the errors of the thickness of the top layer are small, less than 5 per cent.

4.3 HORIZONTAL-FIELD INTERPRETATION

Horizontal magnetic-field and voltage responses of the 300 Ω · m overburden model in Fig. 13 are shown in Fig. 23. The magnetic-field and voltage responses are similar, but opposite in

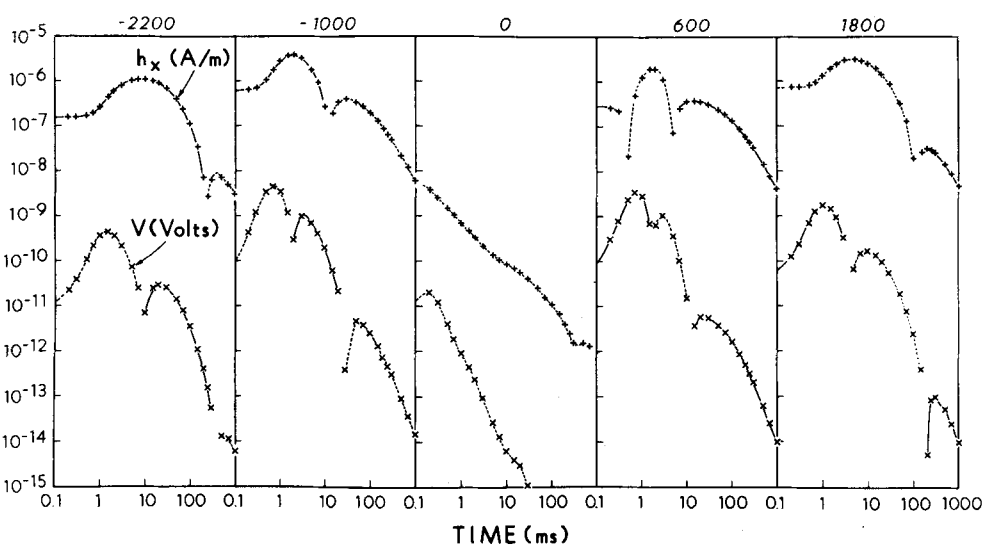

Figure 23. Horizontal magnetic-field and voltage responses (h_x and V_x) for the model of Fig. 13. Solid curves define positive responses and dashed curves define negative responses.

sign, to the magnetic-field and voltage responses of the geothermal model in Fig. 10. This sign change is expected because the models in Figs 4 and 13 represent conductive and resistive structures, respectively.

As expected, the magnetic-field and voltage responses at stations −2200 and −1000 are opposite in sign to the responses at stations 600 and 1800. The weak response at station 0 pinpoints the central position where the overburden is thickest. However, if a sensor were placed 60 m from the centre of any transmitter, a large layered-earth horizontal response would result, which would contaminate the strongest response in Fig. 23 up to and beyond 100 ms. A sensor located at 60 m corresponds to a position that is 10 per cent of the radius of the transmitter. The slow decay of the layered-earth response is caused by the conductive $10\,\Omega \cdot m$ basement in Fig. 13. Thus, horizontal-field measurements can be used to locate and interpret an increase in the thickness of the overburden, but a pinpoint location of the sensor is required. The interpretation of the sign reversals in a magnetic-field and voltage transient in Fig. 23 follow closely the explanation given for the geothermal model in Section 3.3. However, the sign reversals in the magnetic field at stations −1000 and 600 now come earlier in time than at stations −2200 and 1800. This sign reversal pattern is opposite for the geothermal model in Fig. 10.

5 Discussion of results and recommendations

The synthetic data that we presented for inversion and interpretation were optimistic. In practice, transients cannot be interpreted over the time range we have used because of noise considerations at late times and instrumental constraints at early times. However, our results indicate that layered-earth interpretations are not very reliable for estimating the resistivity or depth extent of a 3-D structure. In the few 3-D cases that we presented, we showed that the interpreted section bears no resemblance to the actual 3-D model. The only exception to this was the depth of burial of the 3-D structure.

The depths of burial of 3-D structures can be estimated with layered-earth models. The 3-D structures presented in this paper were all touching the overburden. However, we have studied cases where the structures were detached from their overburdens by 500 m. In these cases we still obtained accurate estimates of the depth of burial.

Fitting models to data calculated from a 3-D, variable-depth, resistive overburden underestimates the depth extent of the 3-D structure. Therefore the maximum thickness of the overburden is underestimated. The 3-D structure representing the lower part of the overburden was replaced with an equivalent layer whose resistivities were less than the resistivity of the overburden. However, layered-earth inversions did produce the correct basement resistivity. In one case where the resistivity of the overburden was $1000\,\Omega \cdot m$, an interpretation based on a ρ_{a_v} data set was very different from that based on a ρ_{a_h} data set. The apparent-resistivity undershoots present in the ρ_{a_v} data caused the addition of a misleading thin conductive layer and resulted in poor estimates of the resistivities of the deeper third layer. The interpretation based on the ρ_{a_h} data resulted in a superior interpretation, because resistivity undershoots in the data were eliminated. The thin conductive layer was absent and all estimates of resistivities and thickness of the second layer were well resolved. This second layer represents the increase in the thickness of the overburden. In some cases we clearly favour using ρ_{a_h} data for 1-D model fitting. However, in other cases model fitting to ρ_{a_h} or ρ_{a_v} data will yield a similar interpretation of a 3-D structure.

A buried 3-D conductor can produce a steep rise in an apparent-resistivity sounding at late times. Therefore, it may not be possible to fit the sounding over the entire time range to a realistic layered-earth model. Truncating the sounding before it starts to rise steeply allows

for a layered-earth fit, an accurate estimate of the depth to the conductor, but results in an overestimate of the conductor's resistivity.

Horizontal-field measurements (magnetic field and voltage) are useful for mapping 3-D structure provided the sensor is located accurately in the centre of the transmitting loop. Magnetic-field and voltage responses calculated exactly at the centres of the transmitting loops peak for stations on the flanks of a 3-D structure, but are very depressed for the station directly over the structure. The depressed responses locate the structure.

Interpretation of central-loop sounding data is greatly assisted by converting vertical magnetic-field and voltage data to apparent resistivity. Such a conversion aids the interpreter in identifying anomalous regions within the geoelectric section. This conversion also provides estimates of layered-earth resistivities required for inversion.

The interpretation of central-loop soundings can be ambiguous because many layered-earth models can be found that fit the data. To reduce some of these non-uniqueness problems, we recommend constraining the interpretation with the known geology and if possible with results from other geophysical methods. When 3-D areas are to be investigated, choose a tight station spacing and measure the horizontal field, because it can indicate lateral resistivity boundaries. Layered-earth models will provide useful information about 3-D geoelectric structure, but do not expect the models to correspond exactly to the true geoelectric section. 3-D forward modelling can also be useful in field investigations, because the responses of suspected 3-D structures can be studied in detail.

Acknowledgments

We are grateful to Frank Frischknecht of the US Geological Survey, Denver Colorado, for making the Vax 11-780 available for this work. Financial support was provided by Amoco Production Co., Arco Oil and Gas Co., Chevron Resources Company, CRA Exploration Pty Ltd, SOHIO Petroleum Co., Unocal Corp., and Utah International Inc., in conjuction with the University of Utah EM Modeling Research Project.

References

Adhidjaja, J. I., Hohmann, G. W. & Oristaglio, M. L., 1985. Two-dimensional transient electromagnetic responses, *Geophysics*, **50**, 2849–2861.

Anderson, W. L., 1975. Improved digital filters for evaluating Fourier and Hankel transform integrals, *NTIS Report PB-242-800.*

Anderson, W. L., 1979. Computer program: Numerical integration of related Hankel transforms of orders 0 and 1 by adaptive digital filtering, *Geophysics*, **44**, 1287–1305.

Anderson, W. L., 1982. Nonlinear least-squares inversion of transient soundings for a central induction loop system (Program NLSTCI), *U.S. geol. Surv. Open File Rep. 82-1129.*

Anderson, W. L. & Newman, G. A., 1985. An album of three-dimensional transient electromagnetic responses for the central-induction loop configuration, *U.S. geol. Surv. Open File Rep. 85-745.*

Anderson, W. L., Frischknecht, F. C., Raab, P. V., Bradley, J. A., Turnross, J. & Buckley, T. W., 1983. Inversion results of time-domain electromagnetic soundings near Medicine Lake, California, geothermal area, *U.S. geol. Surv. Open File Rep. 83-233.*

Bard, Y., 1974. *Nonlinear Parameter Estimation*, Academic Press, New York.

Carnahan, B., Luther, H. A. & Wilkes, J. O., 1969. *Applied Numerical Methods*, John Wiley & Sons, New York.

Dennis, Jr, J. E., Gay, D. M. & Welsch, R. E., 1981. An adaptive nonlinear least squares algorithm, *ACM Trans. math. Softw.*, 7, 348–368.

Draper, N. R. & Smith, H., 1981. *Applied Regression Analysis*, in *Series in Probability and Mathematical Statistics*, John Wiley & Sons, New York.

Eaton, P. A. & Hohmann, G. W., 1986. An evaluation of electromagnetic methods in the presence of geological noise, *Geophysics*, in press.

Fitterman, D. V. & Stewart, M. T., 1986. Transient electromagnetic sounding for groundwater, *Geophysics*, **51**, 995–1005.

Frischknecht, F. C. & Raab, P. V., 1984. Time-domain electromagnetic soundings at the Nevada test site, Nevada, *Geophysics*, **49**, 981–992.

Hohmann, G. W. & Ward, S. H., 1987. Electromagnetic theory for geophysical applications, in *EM volume, Society of Exploration Geophysicists*, in press, The Society of Exploration Geophysicists, Tulsa.

Hoversten, G. M. & Morrison, H. F., 1982. Transient fields of a current loop source above a layered-earth, *Geophysics*, **47**, 1068–1077.

Inman, R. I., 1975. Resistivity inversion with ridge regression, *Geophysics*, **40**, 798–817.

Kaufman, A. A., 1979. Harmonic and transient fields on the surface of a two layer medium, *Geophysics*, **44**, 1208–1217.

Leite, L. W. B. & Leão, J. W. D., 1985. Ridge regression applied to the inversion of two-dimensional areomagnetic anomalies, *Geophysics*, **50**, 1294–1306.

Nabighian, M. N., 1979. Quasi-static transient response of a conducting half-space – an approximate representation, *Geophysics*, **44**, 1700–1705.

Nabighian, M. N., 1982. A review of time-domain electromagnetic exploration: *Proc. Int. Symp. Applied Geophys. in Tropical Regions*, eds Laurenco, J. S. & Rijo, L., Belem, Brazil, September 1–8.

Nabighian, M. N., 1984. Foreword and introduction to special issue of geophysics on time-domain electromagnetic methods of exploration, *Geophysics*, **49**, 849–853.

Newman, G. A., Hohmann, G. W. & Anderson, W. L., 1986. Transient electromagnetic response of a three-dimensional body in a layered-earth, *Geophysics*, **51**, 1608–1627.

Raab, P. V. & Frischknecht, F. C., 1983. Desktop computer processing of coincident and central loop time-domain electromagnetic data, *U.S. geol. Surv. Open File Rep. 83-240.*

Raiche, A. P., 1983. Comparison of apparent resistivity functions for transient electromagnetic methods, *Geophysics*, **48**, 787–789.

Raiche, A. P., Jupp, D. L. B., Rutter, H. & Vozoff, K., 1985. The joint use of coincident loop transient electromagnetic and Schlumberger sounding to resolve layered structures, *Geophysics*, **50**, 1618–1627.

Ryu, J., Morrison, H. F. & Ward, S. H., 1970. Electromagnetic fields about a loop source of current, *Geophysics*, **35**, 862–896.

San Filipo, W. A. & Hohmann, G. W., 1985. Integral equation solution for the transient electromagnetic response of a three-dimensional body in a conductive half-space, *Geophysics*, **50**, 798–809.

Spies, B. R. & Eggers, D. E., 1986. The use and misuse of apparent resistivity in electromagnetic methods, *Geophysics*, **51**, 1462–1471.

Wait, J. R., 1951. The magnetic dipole over the horizontally stratified earth, *Can. J. Phys.*, **29**, 577–592.

Wait, J. R., 1970. *Electromagnetic Waves in Stratified Media*, Pergamon Press, New York.